Published in Physical Review B 61, issue 23, 16213-16222, 2000
which should be used for any reference to this work

Photoemission of bands above the Fermi level: The excitonic insulator phase transition in $1T$-$TiSe_2$

Th. Pillo and J. Hayoz
Institut de Physique, Université de Fribourg, Pérolles, CH-1700 Fribourg, Switzerland

H. Berger and F. Lévy
Institut de Physique Appliquée, Ecole Polytechnique Fédérale, CH-1015 Lausanne, Switzerland

L. Schlapbach and P. Aebi
Institut de Physique, Université de Fribourg, Pérolles, CH-1700 Fribourg, Switzerland

High-resolution angle-resolved photoemission spectroscopy (ARPES) was used to investigate the transition metal dichalcogenide (TMC) $1T$-$TiSe_2$ above and below the phase transition. We find that this system fulfills special conditions such as narrow band width and flat dispersion for bands within $5k_BT$ of the Fermi energy. These prerequisites allow ARPES to observe energy dispersion of bands above E_F without normalization procedures and a leading edge of the Fermi-Dirac distribution cutoff, which is considerably shifted to the unoccupied region with respect to E_F. As a consequence we conclude that the Ti $3d$ band is only thermally occupied at room temperature and considerably shifts towards the occupied range upon cooling. When passing the phase transition, the Se $4p$ bands become backfolded due to new symmetry restrictions. The temperature behavior of the ARPES spectra can, in accordance to transport data, be explained as the occurrence of an excitonic phase suggested by Kohn

I. INTRODUCTION

Angle-resolved photoemission spectroscopy (ARPES) is the cornerstone for mapping occupied energy bands of solids.[1] In a metal or a semimetal, the spectral weight of an ARPES spectrum is cut off by the Fermi-Dirac distribution (f_{FD}), which is inherently temperature dependent. Until quite recently, researchers using ARPES were discouraged to probe electronic states *above* the Fermi energy E_F due to this rapid falloff of spectral weight. Greber *et al.*[2] showed that under special circumstances, thermal population makes electronic states accessible up to $5k_BT$ above E_F.

Mapping electronic bands in a metal or semimetal implies that they cross E_F at some point, i.e., at the Fermi vector $\mathbf{k}_F$, which is a point on the Fermi surface (FS). FS mapping (FSM) experiments using ARPES reveal directly cuts through the FS.[3] More generally, these mapping experiments can be expanded to investigate constant energy surfaces (CES), which can, e.g., be used to elucidate **k**-space locations of valence-band maxima. Straub *et al.*[4] showed recently that one has to be careful in interpreting the data obtained in FSM experiments by probing the FSs of Cu metal [a three-dimensional (3D) system] and the transition metal chalcogenide (TMC) $1T$-$TiTe_2$, a prototype of a two-dimensional (2D) metal. The latter has been proven to be the almost ideal interacting 2D system, i.e., a Fermi liquid.[5] Straub *et al.*[4] further pointed out that for narrow-band systems like $1T$-$TiTe_2$, the FSM does not directly reveal the actual FS, because one has to consider the renormalization of the quasiparticles (QP) in a Fermi liquid, which modifies the momentum distribution $n(\mathbf{k})$. As a consequence, they developed a method to determine accurately the actual Fermi vectors by calculating the 2D gradient of the experimental FSM.

In their case, Straub *et al.*[4] considered metallic systems. Now the question arises what happens in constant energy surface mapping (CESM) experiments near the FS, if the material is weakly semimetallic or even semiconducting with a very small (direct or indirect) band gap of less than $5k_BT$, i.e., when energy bands do not really cross but only graze E_F.

We investigated the subsequent representative of the Ti TMC family, namely $1T$-$TiSe_2$. This material is particularly interesting due to a lattice instability arising around 180–200 K, where a charge density wave (CDW) with a $(2\times2\times2)$ superstructure is formed concurrent with a periodic lattice distortion (PLD).[6,7] Concerning electrical properties, the question whether $1T$-$TiSe_2$ is a semimetal or a semiconductor has led to a number of ARPES contributions,[8–16] which did not lead to a consistent result.

Near E_F properties in $1T$-$TiSe_2$ are governed by two energy bands,[17] namely, the Ti $3d$-derived band around $M(L)$ and the Se $4p$ band around $\Gamma(A)$.[18–26] Anderson *et al.*[8] were the first to show that dispersion effects in the direction perpendicular to the planes, i.e., $k_\perp$, play an important role. They detected holes in the Se $4p$ band at Γ by varying the photon energy and found an overall semimetallic overlap of 120 meV with an occupied Ti $3d$ band at the L point of the unreconstructed Brillouin zone (BZ). Band-structure calculations[18–26] did not help to solve the inconsistencies between Anderson's work[8] and former ARPES data,[12–14] which tended to state clear semiconducting behavior.

Considering the driving force of this second-order CDW phase transition, $1T$-$TiSe_2$ turned out to be, contrary to other $1T$-type layered materials, not the typical representative of a FS nesting material, because there are no large parallel FS

portions. However, DiSalvo *et al.*[6] were the first to suggest a nestinglike model between the Γ-point holes and the L-point electrons. In their model, an electron-phonon interaction would be sufficient to produce a distortion if the electron and hole FSs are near nesting. However, parallel portions on the FS were neither predicted by band-structure calculations[18–26] nor seen by ARPES measurements.[8–16] The second model proposed was an antiferroelectric transition,[27–29] driving soft the corresponding phonon mode. Hereby, the unusually high lattice polarizability ϵ_∞ was the starting point. Another explanation was given by Hughes,[30] who simply considered the lattice coordination, which slightly distorts from octahedral $(1T)$ to trigonal prismatic $(2H)$ as a function of temperature. On the basis of simple total energy arguments, he expected the Ti$3d$ band to shift downwards, therefore lowering the total energy. This band pseudo-Jahn-Teller effect, could, however, not explain the subsidiary spots seen in electron diffraction.[31,32] The most conclusive approach was made by Wilson,[32] who, reviewing experimental data, found evidence for $TiSe_2$ to show an excitonic insulator phase upon decreasing temperature. Such a mechanism was first suggested by Kohn.[33] Even though early photoemission data supported this view,[13,15,16] this picture was questioned by the ARPES works of Anderson and co-workers[8,9] with, though, not very clear arguments. Summarizing, it remains unclear what really happens in $1T$-$TiSe_2$ as a function of temperature. In the present paper, we are looking for further experimental support of one or the other picture.

Using high-resolution ARPES, we find that near L, the Ti$3d$-derived band only appears thermally occupied at room temperature (RT), visible only by thermal excitation of unoccupied states up to $5k_BT$ *above* the Fermi level. Upon cooling, the Ti band shifts to higher binding energies and becomes occupied. Our ARPES data at 120 K reveal, that the Se $4p$ band undergoes a folding due to the doubling of the unit cell and the involved $(2\times2\times2)$ superlattice. From our analysis, we derive a consistent picture of the temperature behavior of $TiSe_2$. The scenario of Kohn's excitonic phases seems the most likely explanation to account for all the observed features.

The paper is organized as follows. The next section deals with the experimental setup and the sample preparation. Section III shows the ARPES results, taken at room temperature (RT) and at 120 K, i.e., in the CDW state. In Sec. IV we shall discuss our results in terms of the aforementioned models and, finally, in Sec. V we summarize our findings.

II. EXPERIMENT

The photoemission experiments were performed in a VG ESCALAB Mk II spectrometer with a base pressure $\leqslant 2\times10^{-11}$ mbar. Our sample goniometer is constructed for motorized computer controlled data acquisition over 2π solid angle[34] and can be cooled with LN_2 down to less than 120 K.[35] X-ray photoelectron spectroscopy was used to check the cleanliness of the sample. The ARPES measurements were performed with He Iα-radiation (21.2 eV) from a high-intensity gas-discharge lamp. The energy resolution was 30 meV and the full angular acceptance cone was less than 1°.

Pure samples of $1T$-$TiSe_2$ were prepared with the chemical vapor transport method.[36] Best samples were grown at 500 °C with ICl_3 as transport agent. These samples showed the best stoichiometry and resistivity ratios $\rho(165\ \mathrm{K})/\rho(295\ \mathrm{K})=3.3$. All samples were grown in the presence of a slight Se excess.[36,37] In addition, Hall coefficient measurements revealed that above the transition at ≈180 K, conduction is p type, i.e., from holes, and below T_c n type, i.e., from electrons[36] in accordance to other measurements.[6] The samples were cut with a blade to the desired shape and mounted with silver epoxy on a polycrystalline Cu sample holder. Sample cleavage was carried out *in situ* using adhesive tape at a pressure in the 10^{-11} mbar range.

After that, they were oriented *in situ* with x-ray photoelectron diffraction (XPD), which provides high-symmetry directions with highest accuracy. Angles can be scanned continuously to perform mappings of intensity at a constant energy such as E_F, or slightly below and above. Briefly, in such a FSM experiment, the spectral function in a small, resolution-limited energy window centered at E_F is scanned over nearly 2π solid angle and represented in a gray scale plot as a function of the polar and the azimuthal angle. This technique is well established and has proven its power in mapping the FS of high T_c cuprates,[38] transition metals,[4,39,40] or of TMCs exhibiting phase transitions.[41] For a review see Ref. 40.

III. RESULTS

In order to get information about the topology of bands near the FS we performed constant energy mapping experiments. Here, we intend to investigate semimetallicity or semiconductivity. Hence, we mapped constant energy surfaces (CES) near E_F and present them in Fig. 1. On the right-hand side, we show CES mappings (CESMs) at three different energies below and above E_F. CESMs are taken with He-I radiation (21.2 eV) at RT. The spectral weight in the energy window is mapped over much of the hemisphere above the sample and represented in a linear gray scale with high intensity corresponding to white. The center denotes normal emission and the outer circle depicts grazing emission. The location of the energy windows with respect to E_F is mimicked on the left-hand side of Fig. 1. The experimental energy resolution was 30 meV, indicated by the width of the energy windows as shown by the gray areas. The Fermi level is depicted as the straight black line whereas the energy positions of the windows are given as the dashed black lines, respectively. Superposed on the bottom CESM is the surface Brillouin zone (SBZ) of the unreconstructed lattice with high-symmetry points indicated. All maps exhibit a trigonal symmetry due to the space group D_{3d}^3 of the $1T$-type TMCs.[17] The intensity difference between the $[\overline{\Gamma M'}]$ and the $[\overline{\Gamma M}]$ azimuths is a matrix element effect and clearly seen as well in FSMs of other $1T$-type TMCs.[4,41]

The two lower maps show three elliptic features around the $\overline{M}$ points of the SBZ and their weaker counterparts around the $\overline{M}'$ points. This spectral weight stems from electrons of the Ti $3d$-derived band. In the isostructural, but metallic, TMC $1T$-$TiTe_2$, these electron pockets can be seen as well around the $\overline{M}$ points.[4] However, the behavior of the pockets here is somewhat puzzling because in the CESM in

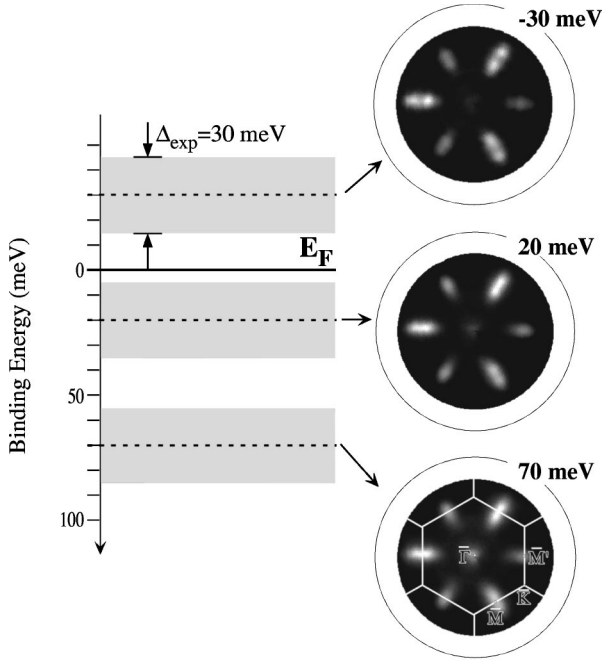

FIG. 1. Constant energy surface mappings of $1T$-$TiSe_2$, performed at room temperature with He-I radiation (21.2 eV). Energy positions are chosen to lie very close *above* and *below* the Fermi energy E_F. Exact location with respect to E_F is sketched in the left part of the figure, together with the width of the energy window from which spectral weight has been mapped.

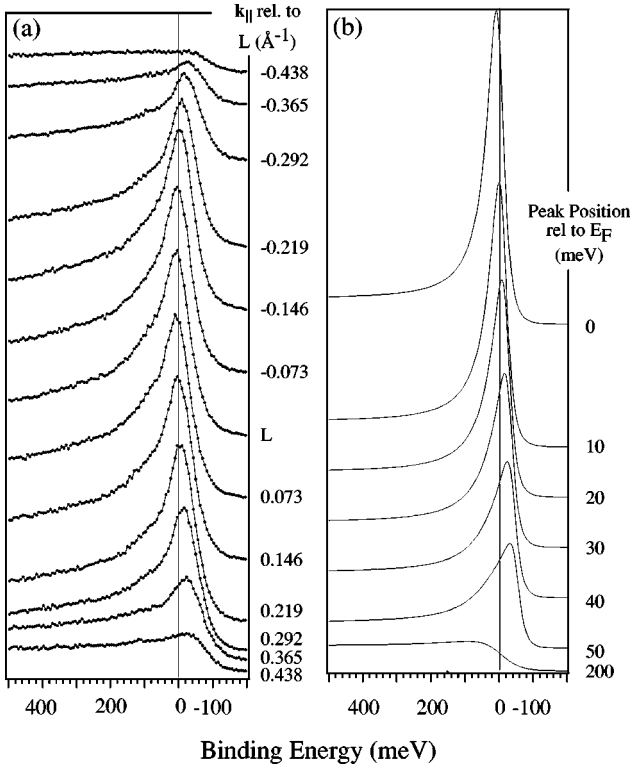

FIG. 2. (a) Angle resolved photoemission (ARPES) spectra in the (ΓALM) plane vs the binding energy, carried out with He-Iα radiation at room temperature. Only spectra near the L point are displayed (see text). (b) Simulation of the ARPES spectra from (a) for varying initial state energy positions (cf. text).

the range above E_F, i.e., at -30 meV binding energy (top panel), this pocket is clearly split into two small circular spots. Furthermore, at 70 meV, these pockets are still clearly visible. This could be interpreted that the Ti $3d$ band is occupied till nearly 100 meV and even below including asymmetry and broadening of the peaks in contrast to other ARPES data.[8,13] So, the case is more complicated and one cannot deduce simply from the CESMs that we have occupied electron pockets around the M points.

Straub *et al.*[4] presented another method to determine the locations of the Fermi level crossings in **k** space for narrow band systems. They carried out FSMs and, afterwards, took the 2D gradient $\nabla_k(\mathbf{k})$ of the experimental pattern. This procedure clearly yields maxima along lines of steepest intensity change around the spots observed in Fig. 1 (not shown). However, using this gradient method only, one cannot distinguish between a band only approaching or really crossing E_F. This point was already stressed in FSMs of isostructural $1T$-TaS_2.[41,42] Therefore, it is necessary to perform ARPES measurements. Yet, ARPES spectra do not evidently reveal the actual peak positions of the spectral function, due to the chopping off of the peaks by the Fermi-Dirac function and/or by small dispersion. To overcome these caveats, a new method has been developed for the cuprates,[43,44] being quasi-2D systems as well. This method is valid under the assumption of particle-hole symmetry near the Fermi level and even overcomes problems due to finite energy *and* momentum resolution as shown by Mesot *et al.*[44] It was published initially to examine the normal state ARPES spectra of underdoped cuprates,[43] and was generalized very recently.[44] It uses the common view to describe ARPES data of quasi-2D systems in terms of the spectral function approach, i.e., the photoemission signal is given by $I(\mathbf{k},\omega) = I_0 A(\mathbf{k},\omega) f(\omega)$, where $A(\mathbf{k},\omega)$ denotes the hole spectral function, $f(\omega)$ the Fermi-Dirac distribution and I_0 the matrix element. Following Mesot *et al.*[44] the symmetrized data, i.e., $I(\omega)+I(-\omega)=\Sigma_k I_0 A(\mathbf{k},\omega)$, can reveal the actual Fermi vector positions, if one assumes particle-hole symmetry near E_F. This method circumvents the above-mentioned problems and one may state whether or not Fermi vectors exist.

We first model our ARPES data with a simple simulation, demonstrating that a large peak lying in the *thermally occupied* region above E_F can also be seen in the spectra above E_F, even in the presence of the Fermi-Dirac cutoff. We then show symmetrized data, clearly indicating that at room temperature no Fermi vector $\mathbf{k}_F$ exists, whereas in the low-temperature phase two Fermi vectors exist directly implying a band that crosses E_F.

We start with our ARPES data and give the results in Fig. 2(a) for the ΓALM high-symmetry plane together with a simulation [Fig. 2 (b)]. The corresponding situation in **k** space is shown in Fig. 3. We plot the BZs for the unreconstructed (1×1) phase as thick rectangles, e.g., $\square L_0' L_1' A_1 L_1 L_0 A_0$. The corresponding low-temperature reconstructed BZs are drawn as the dashed rectangles. Numbers at high-symmetry points give the corresponding BZ. The circular trajectory displays free electron final state vectors for He-I radiation. The work function was measured to be 4.6 eV. The inner potential was chosen as 10 eV as determined experimentally by Anderson *et al.*[8] The line thick-

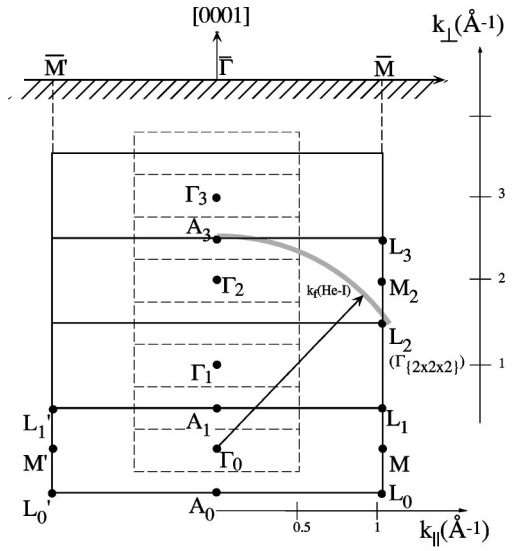

FIG. 3. Sketch of the measurement geometry in **k** space. To calculate the free electron final state vector, given as gray circular trajectory, we assumed an inner potential of 10 eV and measured the work function to be 4.6 eV. Unreconstructed Brillouin zones (BZs) are given as black rectangles, reconstructed BZs are depicted as dashed rectangles. The corresponding surface BZ is given.

ness of the circular trajectroy indicates the covered energy range measured in the ARPES spectra of Fig. 2. As a consequence, the ARPES dispersion plot starts close to the A_3 point and intersects the BZ close to the L_2 point of the BZ.

We come back now to the measurement. In Fig. 2(a) the $\mathbf{k}_\parallel$ distance from the L point is given on the right-hand side of the plot. Most surprisingly, the Ti $3d$-derived band approaches E_F from the unoccupied side till it reaches its minimal modulus of the binding energy at L, in accordance with the theory.[18,19] But, the band never crosses the Fermi level. This is manifest through the fact that the midpoint of the leading edge is shifted substantially to the thermally occupied range of energies above E_F. This finding is very remarkable, because it indicates that a dispersing band up to $5k_BT$ (i.e., 125 meV at 300 K) above the Fermi level can be detected without normalization procedure such as a division by f_{FD} as demonstrated in Ref. 2.

We emphasize that our spectra are given without any data treatment. The reproducibility was checked by several measurements on different charges of samples and different cleavages and after cooling and heating cycles (see below). Spectra always exhibited this peculiar shape. An argument was put forward by Karschnick *et al.*,[45] who detected a sensitive response of the *d*-band intensity due to residual gases. Our working pressure was in the low 10^{-11} mbar range, and we never detected adsorption of residual gases during our measurements, and even after a cooling cycle, valence-band spectra remained unchanged. Therefore, we can definitively rule out contamination effects. The question now remains how the spectra can be explained and what are the approximate peak positions.

To demonstrate effects of narrow and very intense peaks just above E_F on ARPES spectra, we simulated this peak by a Lorentzian (the peak width was estimated to be 30 meV from the room-temperature spectrum at L). For the simulation in Fig. 2(b) we added a constant background to the Lorentzian and multiplied this spectral function with a Fermi-Dirac distribution to account for the thermal cutoff at the Fermi energy.[46] This constant was added to account for an inelastic background, but the asymmetric line shape of the room-temperature spectra may as well have an explanation related to electron-hole fluctuations in the normal state as explained below.

The initial state peak position was set to be the only free parameter. Figure 2(b) shows, from the top to the bottom, the simulated spectra using initial state energies (peak positions of the Lorentzian) varying from 0 meV to 200 meV. From these simulations it is obvious that one may obtain peaks *above* E_F. Several features need to be discussed. First, for an initial state peak position at the Fermi energy (0 meV), the peak is shifted to higher binding energies, i.e., spectral weight peaks at $\approx$10 meV. Already from this result, we may assume that the Ti $3d$ band is only thermally occupied in the measured **k**-space section in Fig. 2(a). Second, up to an initial state energy of 50 meV, the peak is clearly visible and the leading edge is shifted 70 meV into the unoccupied region. Third, only when the Lorentzian reaches 200 meV the spectrum reveals the cutoff at E_F. Between 100 and 200 meV the simulated spectra reveal no longer a distinct peak but the leading edge stays shifted (not shown). This means that up to a $\mathbf{k}_\parallel$ of 0.438 Å^{-1} the Ti $3d$ band lies close (in the range of $5k_BT$) to E_F and considerably affects the spectral line shape. Effective band masses will be discussed below.

We note that it is not intended to give a quantitative analysis of the spectra in terms of the calculation of the spectral function with an appropriate self-energy term, as it was done, e.g., for the Fermi liquid reference compound $1T$-$TiTe_2$.[5] The problem simply is that, to our knowledge, no self-energy is available for this kind of non-Fermi-liquid in our case. We emphasize that there are several conditions to meet such that ARPES can yield this particular spectral shape. As other simulations[47] reveal, such a behavior can only show up if the intrinsic peak width is less than $1/2\times 5k_BT$. Otherwise, the observed peak position lies on the occupied side. Experimentally, this would be reflected solely in a shift of the midpoint of the leading edge, unless, it stays well below the experimental Fermi edge. Another criterion is the finite momentum resolution (<0.07 Å^{-1} in our case). Due to the very small dispersion of the Ti $3d$ band, however, resolution effects can be neglected. The most critical point is the influence of the Fermi-Dirac distribution function. It has been shown for $1T$-$TiTe_2$, that at the actual Fermi vector position, the ARPES spectrum reveals a peak below E_F, whereas it appears above the experimental Fermi energy for higher temperatures.[48] We may overcome this uncertainty by symmetrizing the data (see below).

Actually, the Ti band is *thermally* occupied only. A general statement, however, about the magnitude of an Se $4p$/Ti $3d$-band overlap can only be made if one accounts for the influence of $\mathbf{k}_\perp$ as stressed by Anderson.[8]

Band-structure calculations predict a considerable dispersion of the Se bands from A to Γ,[18,19,22,23] providing a small hole pocket in the vicinity of Γ. With our photon energy we do not have access to this hole pocket because we are located near A and the band maximum is located at Γ. Therefore, we rely on experiments by Anderson *et al.*[8] Using synchrotron radiation to access $\mathbf{k}_\perp$ dispersion they derived a hole pocket

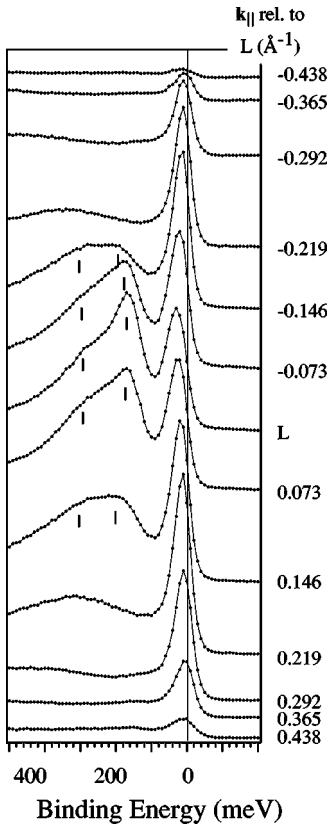

FIG. 4. ARPES spectra analogous to Fig. 2, but at 120 K, i.e., well below the second-order phase transition around 180 K. Only spectra near $L(\Gamma_{2\times2})$ are displayed.

of 15 meV, assuming a constant spin-orbit splitting of the Se $\Gamma_3^- A_3^-$ bands.[26] For the other BZ boundary, i.e., for the Ti $3d$ band we are on the good side, as, in coincidence with theory[18,19] and ARPES data,[8–10] the L point is the point of lowest energy (maximal binding energy) of the Ti $3d$ band.

In the previous paragraph we have observed an thermally occupied Ti $3d$ band close to L with an extremal binding energy of ≈ -10 meV. This is in contrast to published ARPES work,[8–16] which all reported an occupied Ti band. The reason for this is not known. However, this is in agreement with the positive Hall coefficient at RT.[6,36] Altogether with the small hole pocket of 15 meV seen by Anderson, we derive for $1T$-$TiSe_2$ a small semimetallic p-d overlap of ~ 5 meV. We have to emphasize that Anderson's value is estimated and our value is a lower limit. Hence, it is hard to evaluate the overlap precisely. What we can say from our results is that we do neither get a large semimetallic overlap of 120 meV as in other ARPES work[8] nor semiconducting behavior.

Coming back to the measurements of the constant energy surfaces in Fig. 1 we note that neither simply performing CESMs nor taking the 2D gradient allows a final statement about occupied or unoccupied bands. Instead high-resolution ARPES measurements are absolutely necessary to decide whether narrow bands cross E_F or not.

In order to shed light on the underlying mechanism responsible for the CDW formation, we measured the same section in the (ΓALM) plane at 120 K. The results are shown in Fig. 4. From resistivity measurements[36] (Fig. 5) we note that we are still in the decreasing part of the $\rho(T)$ curve.

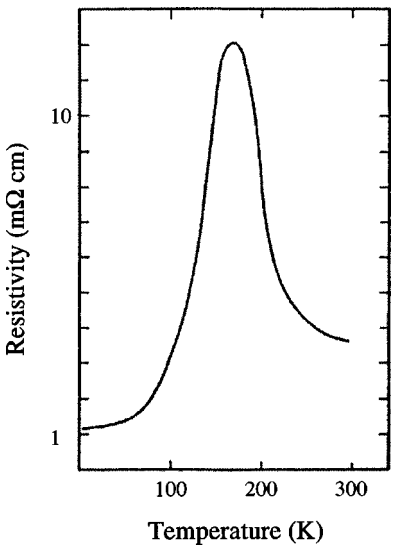

FIG. 5. Measured in-plane ($\perp c$) resistivity $\rho(T)$ as a function of temperature for sample charges used here. For details see text.

Spectra were taken at the same **k**-space locations as in Fig. 2(a). First, one observes a double-peak structure with a hole-like dispersion centered at the L point. The two peaks are indicated by ticks and fade out to weak shoulders upon moving away from L. These two bands, resolved for the first time here, are the backfolded Se $4p$ bands from the A point due to the formation of the $(2\times2\times2)$ PLD superstructure, as already noted by Stoffel *et al.*[13] They could, however, not resolve the two bands. Anderson *et al.*[9] did observe this peak splitting below T_c, although only directly at L.

Second, the Ti $3d$ band, at RT clearly situated above the Fermi level, has now shifted considerably into the occupied region. The maximal binding energy is about $+20$–25 meV, yielding a shift of approximately 30 meV. Note that directly at L, the Se band has more spectral weight than the Ti $3d$ band. This is another indication that we have highly stoichiometric samples following the arguments of the Skibowski group.[8–10]

As mentioned above, the spectral function measured by ARPES does not necessarily yield the actual peak positions. First, the temperature-dependent Fermi-Dirac cutoff may affect the spectra such as to exhibit peaks above E_F at room temperature, which shift below E_F for very low temperatures only by its temperature dependence as previously shown for $1T$-$TiTe_2$.[48] Second, for strong dispersion, actual peak positions can be affected due to the influence of the momentum resolution.

We would like to show now that in our case the Ti $3d$ band only grazes E_F at room temperature, but crosses E_F twice at low temperature. We profit from recent work on quasi-2D materials, where it was suggested that the symmetrization of the electron removal spectrum near E_F leads to conclusive statements about the existence of Fermi crossings (see above). We applied this data analysis on the ARPES spectra of Fig. 2(a) and Fig. 4. The results are shown in Fig. 6. The top panels illustrate the situation of an electron band approaching E_F near the L point and its symmetrized counterpart. In panel Fig. 6(a), the band just grazes E_F, in Fig. 6(b) it is slightly in the unoccupied range, and in Fig. 6(c), the band crosses the Fermi level twice, leading to two clearly

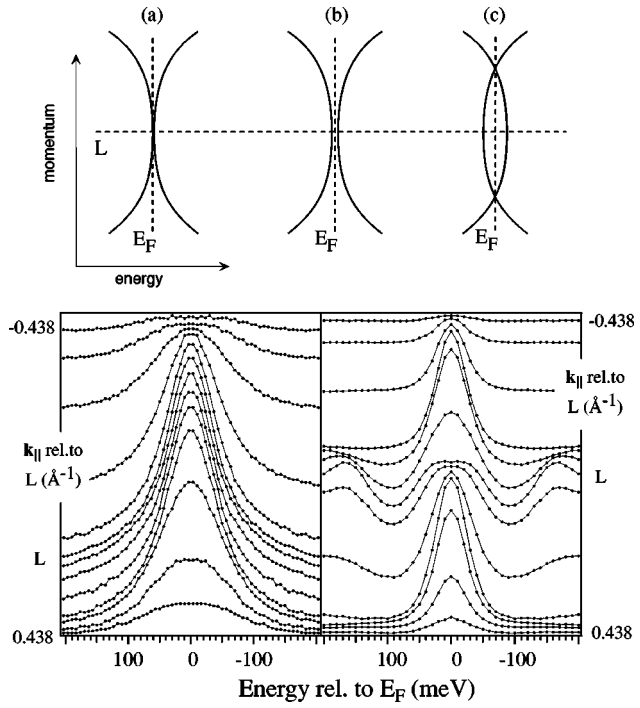

FIG. 6. Top: Sketched situation of a flat band approaching the Fermi level (panel a,b) and crossing E_F (panel c). Bottom: Symmetrized data as obtained from the ARPES spectra of Figs. 2 and 4. The left panel shows the results for room temperature, the right one those for low temperatures. The small bump on both sides of E_F near L in the bottom right panel reflects the backfolded Se $4p$ bands.

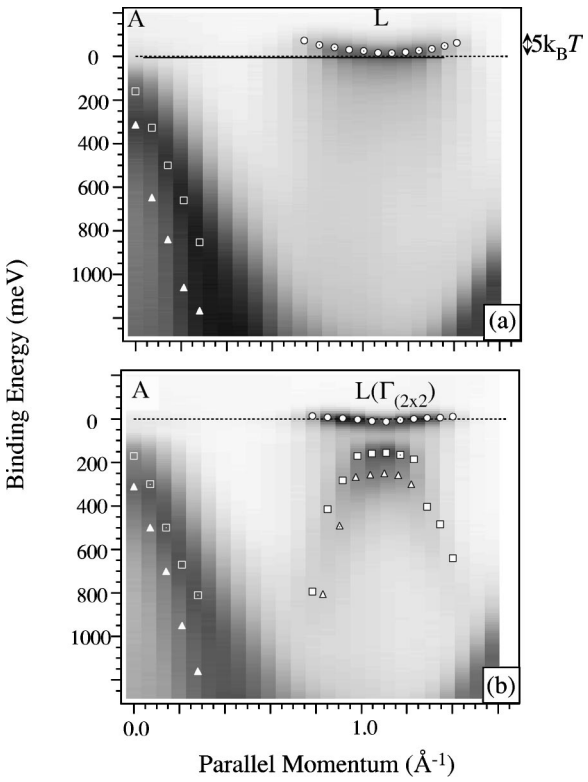

FIG. 7. Complete ARPES sets for the (ΓALM) plane, taken with 21.2 eV photons at room temperature (a) and at 120 K (b). In (a), the region of thermally excited electrons *above* E_F is depicted. Modelled peak positions are superposed for the Ti $3d$ bands ($\odot$) as well as for the Se $4p$ bands ($\triangle$,$\square$) at the respective temperatures.

distinguishable Fermi vectors. The bottom panels show the symmetrized data for room temperature (left) and for 120 K (right). Data is shown for the same momentum range as in Figs. 2 and 4. For room temperature one observes a peak evolving upon approaching the L point, but this shape shows no dip in the vicinity of L, as it would be the case, if the peak crossed E_F.[43,44] Completely different are the data of the bottom right panel for low temperature. Here, a peak evolves, gets maximum intensity, then decreases considerably in intensity, at the same time yielding a small but visible dip at the L point, before it reappears again upon moving away from the L point to the other direction. This, if following the arguments of Mesot *et al.*[44] is a clear indication that at low temperatures the Ti $3d$ band crosses the Fermi level twice, or, in other words, one has occupied states. At room temperature, however, the Ti $3d$ band only grazes but does *not* cross E_F, or, in other words, the band is only thermally occupied. From the fact that we see a symmetric peak evolving at room temperature (bottom left panel), we conclude that the Ti $3d$ band in fact approaches E_F rather closely and we can estimate the maximal binding energy at the L point to be approximately 5–10 meV, if comparing with our simulation.

In order to be able to understand the temperature behavior of the Se and Ti bands, we have to consider band masses and possible band interaction. Therefore, we present in Fig. 7 the complete set of ARPES spectra in the (ΓALM) plane, starting at the A point. Spectra were obtained at RT [Fig. 7(a)] and at 120 K in the CDW phase [Fig. 7(b)]. Energy and momentum axes are extendend in comparison to the ARPES spectra in Figs. 2 and 4. The data are shown in a linear gray scale representation with maximum intensity corresponding to black. The Fermi level is given by the black dashed line. In Fig. 7(a), the energy range *above* E_F, which is thermally populated, is indicated by the arrow. The high-symmetry points A and L are given, meaning that we start from a polar emission angle $\Theta_{Vac}=0°$ going down to higher polar angles up to $\Theta_{Vac}=50°$. The ARPES spectra have been mapped onto a regular $\mathbf{k}_\parallel$ grid, obeying the usual photoemission formula[1]

$$\mathbf{k}_\parallel(\text{Å}^{-1}) = 0.512\sqrt{h\nu(\text{eV}) - |E_{Bin}|(\text{eV}) - |\phi|(\text{eV})}\sin\Theta_{Vac} \quad (1)$$

with $h\nu$, E_{Bin}, and ϕ denoting the photon energy, the binding energy, and the sample work function (4.6 eV in our case), respectively.

In the low-temperature plot [Fig. 7(b)] the new center of the reconstructed BZ $\Gamma_{(2\times2)}$ is marked, which corresponds to the old L point due to the in-plane (2×2) reconstruction. To evaluate the dispersion and band masses we fitted the spectra to model functions, which consisted of two Lorentzians for the case of the Se bands near the A point, of one Lorentzian for the RT Ti band around L (see simulation above), and of three Lorentzians around L in the CDW phase. All model functions included a constant background and the Fermi-Dirac distribution. The results of the peak fits are superposed on the ARPES spectra. The circles ($\odot$) denote the Ti $3d$ bands, the triangles $\triangle$ (hollow and filled) and the squares $\square$ (hollow and filled) depict the Se $4p$ bands, i.e., the $\Gamma_3^- A_3^-$

band and its spin-orbit split partner. The uppermost Se band at A is the one which crosses the Fermi level upon approaching Γ according to Anderson *et al.*[8] The backfolded bands in the CDW phase exhibit almost identical effective masses as the Se $4p$ bands around A and also the same splitting. Therefore, the assignment to the (2×2) reconstructed Se bands is straightforward and in perfect agreement with published data.[13] Importantly, the Se bands do not shift in energy upon cooling as the Ti band obviously does.

A polynomial fit (order 2) to the bands in $\mathbf{k}_\parallel$ for the RT data yields the band masses to be of the order of 8.8 $\pm5\%m_0$, with m_0 being the mass of a free electron, for the Ti $3d$ bands, i.e., the electron bands, and $0.55\pm5\%m_0$ for the hole (Se $4p$) bands. The latter value is in good agreement with published results.[13] It is puzzling that the backfolded Se bands display a flattened dispersion in the vicinity of the $\Gamma_{(2\times2)}$ point. This is a possible hint to band interaction between the Ti electron and the Se hole bands as discussed below.

IV. DISCUSSION

In this section we shall discuss the results shown in Sec. III in terms of the in-plane ($\perp$ c) resistivity ρ (Fig. 5) and the underlying mechanism for the PLD transition. The curve is valid for the sample charges we measured and was published earlier (taken from Ref. 36). One observes that the background resistivity shows metallic behavior and that a broad hump is superimposed, which extends from room temperature down to below 100 K. The reason for this hump is unclear up to now. The only thing one knows is that it can be suppressed by metal or chalcogen doping as shown by early transport work.[7,36,37] The resistivity ratio $\rho(165\ K)/\rho(295\ K)$ equals 3.3 and agrees with other published data (see Ref. 36 and references therein). Measurements of the Hall coefficient indicate that the majority of carriers at RT are holes and that well below the transition the conduction is prominently electronic.[7,36] So, stoichiometric samples are p-type conductors.[49]

To recapitulate, $1T$-$TiSe_2$ is (semi)metallic for high temperature and (semi) metallic at low temperature. However, in between, a state with a higher resistivity exists. Therefore the Fermi surface must be affected in this temperature range and should yield another shape for temperatures below $T_c \approx 200$ K than for RT. If one compares the results of the transport measurements with our ARPES results, one observes astonishingly good qualitative agreement. At RT, the Ti $3d$ band is thermally occupied and conductivity must stem from the Γ point holes of the Se band. Below T_c, however, the Ti $3d$ band is shifted towards the occupied range and, hence, generates a real electronlike Fermi surface with actual crossings of E_F. The smaller resistivity at low temperature and the negative Hall coefficient can be explained by an electron-hole instability, which was originally introduced by Mott.[50] He considered a semimetal with a small number of electrons and holes and noticed the following: If the number of carriers is sufficiently small, the screening of the Coulomb interaction between electrons and holes is weak. However, an unscreened Coulomb interaction will always lead to a weakly bound electron-hole pair, i.e., an exciton. This model of the *excitonic insulator* was developed

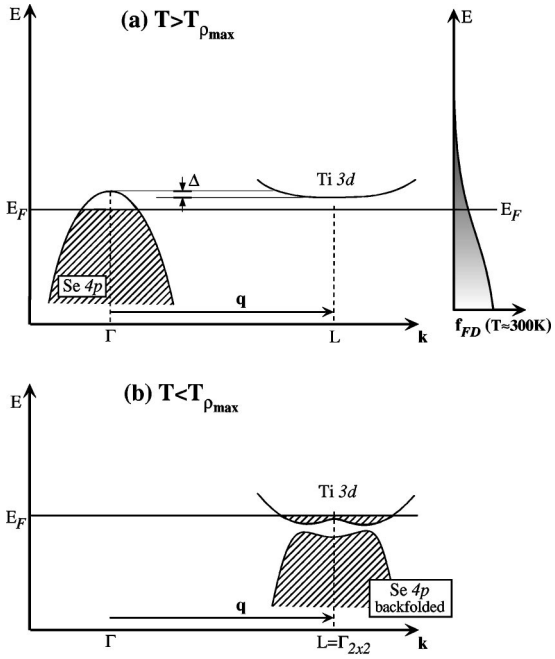

FIG. 8. Sketch for the occurrence of an excitonic insulator phase according to Kohn:[33] (a) situation before the phase transition ($T > T_{\rho_{max}}$) and (b) the situation after the second-order phase transition for $T < T_{\rho_{max}}$, implying the required $(2\times2\times2)$ reconstruction, corresponding to the spanning (not nesting) vector $\mathbf{q}$. Δ yields the indirect gap (negative or positive) of the electron and hole bands (see text).

theoretically by Knox,[51] des Cloiseaux,[52] Keldysh,[53] and excellently reviewed by Halperin and Rice.[54] Kohn showed[33] that in the case of a semimetal or semiconductor with a small indirect (negative or positive) band gap, excitonic phases may occur under several conditions.

First, there has to be a reconstruction that doubles the periodicity of the lattice.[33,54] In $TiSe_2$, in fact, the phase transition is accompanied by a PLD leading to a $(2\times2\times2)$ reconstruction. This first prerequisite is therefore fulfilled. The second condition is the very existence of two bands, an electron band and a hole band at different locations in $\mathbf{k}$ space with an indirect gap as argued by Kohn.[33] The situation is sketched in Fig. 8 for a semimetallic phase. In our case the Se$4p$ band is partly unoccupied. The dashed area denotes the occupied part and the horizontal line denotes the Fermi level, respectively. At the L point, the Ti $3d$ band has its energy minimum slightly above E_F. The resulting overlap Δ, in this case, equals 5 to 10 meV. The vector spanning $\mathbf{k}$ space from Γ to L yields exactly the value of a reduction by 2 in each direction, i.e., it corresponds to the $(2\times2\times2)$ reconstruction. This is the situation for $T > T_{\rho_{max,}}$ where $T_{\rho_{max}}$ corresponds to that temperature where the resistivity is maximal. In addition we display at the right a Fermi-Dirac distribution f_{FD} for $T \approx 300$ K in order to visualize the extent of the band filling with respect to thermal population. $T_{\rho_{max}}$ is not significant (see below). However, $T_c \approx 200$ K is significant for the phase transition (PLD). In general, $T_{\rho_{max}} < T_c$, but $T_{\rho_{max}}$ strongly depends on impurities or defects.[36,37] In the case of $T < T_{\rho_{max}}$ [Fig. 8(b)], the Se $4p$ band at Γ is unperturbed as shown in Fig. 7. The situation at L, or in other words at

$\Gamma_{(2\times2)}$, has dramatically changed. The Se $4p$ is backfolded and the Ti $3d$ band is shifted down. The experimentally observed situation is in perfect agreement with the picture presented by Kohn for the occurrence of the excitonic phase.[33]

We can estimate the binding energy of a Mott-Wannier exciton and compare it to the band overlap Δ. The exciton binding energy in electron volts is given by:[54]

$$E_B^{exc} = \frac{\mu}{m_0}\frac{1}{\epsilon^2}\ (13.6)\ \text{eV} \tag{2}$$

with μ denoting the reduced effective exciton mass given by $1/\mu = 1/m_h + 1/m_e$. Here, m_e and m_h are the effective masses of the electron and hole bands, respectively whereas m_0 is the free electron rest mass. ϵ is the dielectric constant. Introducing the experimental values, we obtain a formula for the exciton binding energy:

$$E_B^{exc} = 0.52\frac{1}{\epsilon^2}\ (13.6)\ \text{eV} = \frac{7.04}{\epsilon^2}\ \text{eV}. \tag{3}$$

For the dielectric constant no exact values ϵ exist. Liang *et al.*[27] have measured the lattice polarizability $\epsilon_\infty = 36$, which would yield a value of 5.5 meV for the exciton binding energy.

Besides, Zittartz[55] found a relation, using the Hartree-Fock approximation, between the transition temperature for the excitonic phase, $T_c|_{\Delta(T_c)=0}$, and the exciton binding energy:

$$k_B T_c|_{\Delta(T_c)=0} = C E_B^{exc}. \tag{4}$$

Hereby, C is a dimensionless factor depending on the band masses. T_c has been chosen to be 200 K as a lower limit (see below). In the isotropic case, i.e., $m_e = m_h$, C equals 1.4. This would yield an exciton binding energy of $E_B^{exc} \approx 11$ meV. As hole and electron bands are not isotropic, but yield different effective masses, we find for C a value of 1. This gives $E_B^{exc} \approx 17$ meV.

With Eq. (3), a binding energy of roughly 17 meV would yield a dielectric constant $\epsilon = 20$. This number is similar to that of isostructural $1T$-TiS_2,[56] which is accepted to be a semiconductor.[57–59] However, recent *ab initio* calculations[18,60] claim that $1T$-TiS_2 is semimetallic as well. Keeping this in mind, the value of $\epsilon_\infty = 36$ as stated by Liang has to be questioned with respect to its validity to use here.

Our estimation (Fig. 8) for the overlap Δ is roughly 0 to 5 meV. This is reasonable, if one considers that the value for the hole band, 15 meV, is an estimation based on the argument of constant spin-orbit splitting over a large $\mathbf{k}$ range.[26] Transport data[36] suggest that one has free carriers with positive Hall coefficient, i.e., holes at RT. A *p*-type conduction at RT means that the hole concentration n_h is larger than the electron concentration n_e. As shown above the Ti $3d$ band is only thermally populated by electrons leaving only a small number of electrons to form excitons. These might give rise to fluctuations at RT and are, actually, seen in ARPES.[9] The result is, that at RT, the system is already in an excitonic state. We only detect a large asymmetry of the Ti $3d$ band but no distinct shoulders as in Ref. 9. Nonetheless, the spectral function may include excitonic fluctuation effects what would cause this asymmetry.

Lowering the temperature, the Ti $3d$ band starts to shift slightly to larger (positive) binding energies. A reason may be the lattice distortion, which removes the degeneracy of the metallic bands due to symmetry changes of the crystal field from octahedral towards trigonal prismatic coordination. It is equivalent to Hughes' argument[30] of a band pseudo-Jahn-Teller effect. We have to remember that all octahedrally coordinated effect TMCs undergo small lattice distortions as a function of temperature.[61] But not each TMC shows an instability, as for instance, $TiTe_2$,[5] TiS_2,[11] and $TaTe_2$.[62] Therefore, one might guess a possible Jahn-Teller effect at the starting point of lattice distortions in these materials. However, the TMCs are not simple ionic crystals and correlation effects influence the possible instabilities. For example, the properties of $1T$-TaS_2 appear affected already at RT by the Mott localization transition at 180 K,[41] and in some $2H$ polytypes, a saddle band mechanism based on the model by Scott and Rice[63] has been recently discussed.[64,65]

The formation of more electron-hole pairs due to the shift of the Ti $3d$ band also contributes to the gain in energy. Fluctuations due to the excitonic phase occurring already at RT are consistent with the increase of resistivity with decreasing temperature below 300 K. At $T = T_{\rho_{max}}$ the Ti $3d$ band reaches a position where $n_h = n_e$. The number of excitons and also the resistivity is maximal. The temperature of maximal resistivity is not menaningful but only defines a lower limit for formula (4). Upon further decreasing the temperature the Ti $3d$ band continues shifting, generating electrons in excess, which are responsible for the decreasing resistivity and a negative Hall coefficient. Resistivity can also be further decreased by a reduced relaxation rate due to the lower temperature. As long as $|\Delta| \leqslant E_B^{exc}$,[33] Mott-Wannier excitons are present with large radii and free carriers are removed from the Fermi surface. The instability extends over a large temperature range and a metallic character appears at lower temperatures, below about 100 K.

A last point to mention is the flatter dispersion of the backfolded Se $4p$ bands near the apex. This is due to simple band interaction leading to a Wilson band gap. A band-structure calculation[24] for the distorted phase based on the model of Yoshida[66] for the electronic susceptibility who carried out a tight-binding fit to Zunger's LDA calculation[19] provides rather good agreement upon comparison to our low-temperature data.

In summary, we argue that $1T$-$TiSe_2$ exhibits a Kohn excitonic phase extended on a wide temperature interval as shown by angle-resolved photoemission and the comparison to transport data. Nevertheless, $1T$-$TiSe_2$ is an exception to the rule in the TMCs as it shows a second-order phase transition. To our experience, there is no other TMC that shows such a temperature behavior. Therefore, other octahedral ($1T$) and trigonal prismatic ($2H$) TMCs may be explained by more conventional mechanisms based on Fermi surface nesting or saddle bands.

V. SUMMARY

Using high-resolution ARPES as a function of temperature to investigate the TMC $1T$-$TiSe_2$, we were able to show

two aspects. With respect to ARPES as a technique, we demonstrated that without normalization procedures it is possible to see *unoccupied* energy bands in photoemission if prerequisites such as narrow band width and flat dispersion are met. The leading edge of a photoemission spectrum may then be well shifted within the $5k_BT$ limit set by the Fermi-Dirac statistics.

Being aware of this possibility we were able to show that the Ti $3d$ band in the TMC $1T$-$TiSe_2$ considerably shifts towards the occupied range. When passing the phase transition, the Se $4p$ bands become backfolded due to the periodic lattice distortion. The temperature behavior can be explained as the occurrence of a Kohn excitonic phase, consistently with transport data.

ACKNOWLEDGMENTS

We wish to thank L. Degiorgi for many helpful discussions and for the reading of the manuscript. We are greatly indebted to our workshop and electric engineering team, including O. Raetzo, E. Mooser, O. Zosso, R. Schmid, R. Vonlanthen, Ch. Neururer, and F. Bourqui. Financial support by the Fonds National Suisse pour la Recherche Scientifique is gratefully acknowledged.

[1] S. Hüfner, *Photoelectron Spectroscopy* (Springer, New York, 1995).
[2] T. Greber, T.J. Kreutz, and J. Osterwalder, Phys. Rev. Lett. **79**, 4465 (1997).
[3] P. Aebi, J. Osterwalder, R. Fasel, D. Naumović, and L. Schlapbach, Surf. Sci. **307-309**, 917 (1994).
[4] Th. Straub, R. Claessen, P. Steiner, S. Hüfner, V. Eyert, K. Friemelt, and E. Bucher, Phys. Rev. B **55**, 13 473 (1997).
[5] R. Claessen, R.O. Anderson, J.W. Allen, C.G. Olson, C. Janowitz, W.P. Ellis, S. Harm, M. Kalning, R. Manzke, and M. Skibowski, Phys. Rev. Lett. **69**, 808 (1992).
[6] F.J. DiSalvo, D.E. Moncton, and J.V. Waszczak, Phys. Rev. B **14**, 4321 (1976).
[7] F.J. DiSalvo and J.V. Waszczak, Phys. Rev. B **17**, 3801 (1978).
[8] O. Anderson, R. Manzke, and M. Skibowski, Phys. Rev. Lett. **55**, 2188 (1985).
[9] O. Anderson, G. Karschnick, R. Manzke, and M. Skibowski, Solid State Commun. **53**, 339 (1985).
[10] O. Anderson, W. Drube, G. Karschnick, and M. Skibowski, Ann. Isr. Phys. Soc. **6**, 315 (1983).
[11] R.Z. Bachrach, M. Skibowski, and F.C. Brown, Phys. Rev. Lett. **37**, 40 (1976).
[12] C.H. Chen, W. Fabian, F.C. Brown, K.C. Woo, B. Davies, B. DeLong, and A.H. Thompson, Phys. Rev. B **21**, 615 (1980).
[13] N.G. Stoffel, S.D. Kevan, and N.V. Smith, Phys. Rev. B **31**, 8049 (1985).
[14] N.G. Stoffel, F. Lévy, C.M. Bertoni, and G. Margaritondo, Solid State Commun. **41**, 53 (1982).
[15] M.M. Traum, G. Margaritondo, N.V. Smith, J.E. Rowe, and F.J. DiSalvo, Phys. Rev. B **17**, 1836 (1978).
[16] G. Margaritondo, C.M. Bertoni, J.H. Weaver, F. Lévy, N.G. Stoffel, and A.D. Katnani, Phys. Rev. B **23**, 3765 (1981).
[17] J.A. Wilson and A.D. Yoffe, Adv. Phys. **18**, 193 (1969).
[18] C.M. Fang, R.A. De Groot, and C. Hass, Phys. Rev. B **56**, 4455 (1997).
[19] A. Zunger and A.J. Freeman, Phys. Rev. B **17**, 1839 (1978).
[20] H. Isomäki and J. von Boehm, J. Phys. C **14**, L75 (1981).
[21] H. Isomäki, J. von Boehm, and P. Krusius, J. Phys. C **12**, 3239 (1979).
[22] E. Pehlke, W. Schattke, O. Anderson, R. Manzke, and M. Skibowski, Phys. Rev. B **41**, 2982 (1990).
[23] E. Pehlke and W. Schattke, Solid State Commun. **69**, 419 (1989).
[24] N. Suzuki, A. Yamamoto, and K. Motizuki, Solid State Commun. **49**, 1039 (1984).
[25] J. von Boehm and H.I. Isomäki, J. Phys. C **15**, L733 (1982).
[26] J. von Boehm and H.I. Isomäki, Phys. Rev. B **24**, 6945 (1981).
[27] W.Y. Liang, G. Lucovsky, J.C. Mikkelsen, and R.H. Friend, Philos. Mag. B **39**, 133 (1979).
[28] W. Y. Liang, in *Physics and Chemistry of Electrons and Ions in Condensed Matter*, edited by J. V. Acrivos *et al.* (Reidel, Dordrecht, 1984), pp. 459.
[29] R.M. White and G. Lucovsky, Nuovo Cimento Soc. Ital. Fis., B **38**, 280 (1977).
[30] H.P. Hughes, J. Phys. C **10**, L319 (1977).
[31] J.A. Wilson and S. Mahajan, Commun. Phys. **2**, 23 (1977).
[32] J.A. Wilson, Phys. Status Solidi B **86**, 11 (1978).
[33] W. Kohn, Phys. Rev. Lett. **19**, 439 (1967).
[34] J. Osterwalder, T. Greber, S. Hüfner, and L. Schlapbach, Phys. Rev. B **44**, 13 764 (1991).
[35] E. Boschung, Th. Pillo, J. Hayoz, L. Patthey, P. Aebi, and L. Schlapbach, Phys. Rev. B **58**, R10 210 (1998).
[36] F. Lévy and Y. Froidevaux, J. Phys. C **12**, 473 (1979).
[37] F. Lévy, J. Phys. C **12**, 3725 (1979).
[38] P. Aebi, J. Osterwalder, P. Schwaller, L. Schlapbach, M. Shimoda, T. Mochiku, and K. Kadowaki, Phys. Rev. Lett. **72**, 2757 (1994).
[39] P. Aebi, T.J. Kreutz, J. Osterwalder, R. Fasel, P. Schwaller, and L. Schlapbach, Phys. Rev. Lett. **76**, 1150 (1996).
[40] J. Osterwalder, Surf. Rev. Lett. **4**, 391 (1997).
[41] Th. Pillo, J. Hayoz, H. Berger, M. Grioni, L. Schlapbach, and P. Aebi, Phys. Rev. Lett. **83**, 3494 (1999).
[42] Th. Pillo, J. Hayoz, H. Berger, L. Schlapbach, and P. Aebi (unpublished).
[43] M.R. Norman, H. Ding, M. Randeria, J.C. Campuzano, T. Yokoya, T. Takeuchi, T. Takahashi, T. Mochiku, K. Kadowaki, P. Guptasarma, and D.G. Hinks, Nature (London) **392**, 157 (1998).
[44] J. Mesot, A. Kaminski, H.M. Frettwell, M. Randeria, J.C. Campuzano, H. Ding, M.R. Norman, T. Takeuchi, T. Sato, T. Yokoya, T. Takahashi, I. Chong, T. Terashima, M. Takano, T. Mochiku, K. Kadowaki, e-print, cond-mat/9910430.
[45] G. Karschnick, O. Anderson, W. Drube, and M. Skibowski, Surf. Sci. **155**, 46 (1985).
[46] The effective temperature for f_{FD} accounting for the sample temperature (RT) and the instrumental resolution has been obtained from a fit of a Fermi edge of the polycrystalline Cu sample holder.
[47] Th. Pillo (unpublished).
[48] R. Claessen (private communication).
[49] J.A. Wilson, A.S. Barker, Jr., F.J. Di Salvo, Jr., and J.A. Ditzen-

berger, Phys. Rev. B **18**, 2866 (1978).
[50] N.F. Mott, Philos. Mag. **6**, 287 (1961).
[51] R.S. Knox, Solid State Phys. Suppl. **5**, 100 (1963).
[52] J. des Cloiseaux, J. Phys. Chem. Solids **26**, 259 (1965).
[53] L.V. Keldysh and Y.V. Kopaev, Fiz. Tverd. Tela (Leningrad) **6**, 2791 (1965) [Sov. Phys. Solid State **6**, 2219 (1965)].
[54] B.I. Halperin and T.M. Rice, Rev. Mod. Phys. **40**, 755 (1968).
[55] J. Zittartz, Phys. Rev. **162**, 752 (1967).
[56] G. Lucovsky, R.M. White, W.Y. Liang, and J.C. Mikkelsen, Philos. Mag. B **34**, 907 (1976).
[57] R.H. Friend, D. Jérome, W.Y. Liang, J.C. Mikkelsen, and A.D. Yoffe, J. Phys. C **10**, L705 (1977); R.H. Friend, D. Jérome, and A.D. Yoffe, *ibid.* **15**, 2183 (1984); J.J. Barry, H.P. Hughes, P.C. Klipstein, and R.H. Friend, *ibid.* **16**, 393 (1983); M. Schärli, J. Brunner, H.P. Vaterlaus, and F. Lévy, *ibid.* **16**, 1527 (1983).
[58] D.R. Allan, A.A. Kelsey, S.J. Clark, R.J. Angel, and G.J. Ackland, Phys. Rev. B **57**, 5106 (1998).
[59] T. Matsushita, S. Suga, A. Kimura, H. Negishi, and M. Inoue, Phys. Rev. B **60**, 1678 (1999).
[60] S. Sharma, T. Nautiyal, G.S. Singh, S. Auluck, P. Blaha, and C. Ambrosch-Draxl, Phys. Rev. B **59**, 14 833 (1999).
[61] J.A. Wilson, F.J. Di Salvo, and S. Mahajan, Adv. Phys. **24**, 117 (1975).
[62] Th. Pillo (unpublished).
[63] T.M. Rice and G.K. Scott, Phys. Rev. Lett. **35**, 120 (1975).
[64] R. Liu, C.G. Olson, W.C. Tonjes, and R.F. Frindt, Phys. Rev. Lett. **80**, 5762 (1998).
[65] Th. Straub, Th. Finteis, R. Claessen, P. Steiner, S. Hüfner, P. Blaha, C.S. Oglesby, and E. Bucher, Phys. Rev. Lett. **82**, 4504 (1999).
[66] Y. Yoshida and K. Motizuki, J. Phys. Soc. Jpn. **49**, 898 (1980).